JOURNAL OF MATERIALS SCIENCE 30 (1995) 5073–5077

# Low-cycle fatigue of polycrystalline α-iron modified by mutually immiscible silver-ion implantation

H. W. WANG
*Corrosion and Protection Centre, University of Manchester Institute of Science and Technology, P.O. Box 88, Manchester M60 1QD, UK*

D.Z. YANG, W.D. SHI
*Department of Materials Engineering, Dalian University of Technology, Dalian 116024, People's Republic of China*

S. PATU
*The State Key Laboratory for Fatigue and Fracture of Materials, Institute of Metal Research, Academia Sinica, Shenyang 110015, People's Republic of China*

Cyclic deformations of annealed pure polycrystalline α-iron with and without further mutually immiscible silver-ion implantation (90 keV, $6 \times 10^{16}$ ions $cm^{-2}$) were studied in a plastic strain-controlled tension–compression fatigue test (triangular loading waveform, frequency 0.02–0.3 Hz, and plastic strain range $3 \times 10^{-3} - 1.2 \times 10^{-2}$). The obtained plastic strain-life ($\Delta\varepsilon_p$–$N_f$) curves showed that the iron specimens could survive for a greater number of cycles before failure when implanted. Comparison of the cyclic stress–strain curves suggested that the implanted specimens had maintained a relatively more stable microstructural change than those unimplanted ones which had undergone a violent cyclic hardening during cyclic deformation. This is proposed to be a strong indication that the fatigue ductility has been improved and the cross slip of screw dislocations, which leads to the evolution of the persistent slip bands for fatigue damage, was hindered to some extent after ion implantation.

## 1. Introduction

In a previous paper [1], it was demonstrated that the high-cycle fatigue (HCF) endurance limit stress of polycrystalline α-iron could be increased by 3.7%–6.4% in the dose range $1–10 \times 10^{16}$ ions $cm^{-2}$ metallic silver-ion implantation. It was proposed that enhanced implantation radiation-induced defects and super solid-solution strengthening were the dominant mechanisms for property improvement, although iron and silver are thermodynamically mutually immiscible [2].

HCF tests are generally conducted in a stress-control mode. Because of the characteristic high-frequency (a few tens of Hertz) and low-stress (usually smaller than the yield stress, $\sigma_{0.2}$) test conditions, HCF tests are habitually adopted to measure the stress–life relationship, termed the Wöler or *S–N* curve. However, strain-controlled, and especially plastic strain-controlled, low-cycle fatigue (LCF) tests are more valid in the evaluation of fatigue damage behaviour and the dislocation plasticity of metallic crystals [3–10]. Engineering materials and structures in service often still suffer from severe low-frequency and high-loading conditions.

On the other hand, ion implantation as a low-temperature, non-equilibrium processing technique, has been verified to be capable of producing beneficial effects on the reduction of wear [11, 12], corrosion [13], and high-temperature oxidation [14]. Those as-published reports on face-centred cubic (fcc) metals showed that ion implantation could also be applied to improve fatigue properties of fcc metals, either by microalloying and strengthening of the surface, or by stacking fault energy (SFE) lowering mechanisms [15–19]. As a result, surface emergence of subsurface developing persistent slip bands (PSBs) could be either prohibited or homogenized. Because surface sites, where PSBs emerge, are the surface irregularities for the stress concentration and, therefore, intrinsic sites for preferential initiation of fatigue cracks, provided that there are no extrinsic crack nucleation sites caused by insufficient surface smoothness, it is thus reasonably expected that the fatigue crack initiation (FCI) life may be increased by ion implantation.

Silver and iron are mutually immiscible in both a high-temperature liquid state and a low-temperature solid state by the thermodynamical equilibrium criterion [2]. However, they can be expected to be mixed, on an atomic scale, by implantation. In this report, LCF test results are reported on the cyclic stress response to strain, cyclic saturation stress-strain relation, and strain–life relation for polycrystalline α-iron,

0022–2461 

with and without silver-ion implantation. Proposed mechanisms for this ion-implantation modification of LCF behaviour are also presented.

## 2. Experimental procedure

Pure polycrystalline α-iron (Armco iron, total impurity content less than 0.1 wt%) was chosen as the substrate material from which all specimens were made. Fig. 1 shows the geometry and dimensions of LCF specimens. Before implantation, these specimens were first annealed at 600 °C for 1 h, followed by careful manual grinding and polishing with diamond paste, and finished with electropolishing in a solution of 10% perchloric acid in ethanol at − 20 °C. The average chemical composition of the substrate and the detailed treatment before implantation can be found elsewhere [1].

Metallic silver-ion implantation was conducted on an ion-implantation system with a metallic evaporation vapour vacuum arc (MEVVA) type of ion source. The implantation was proceeded at a working vacuum of $10^{-6}$ torr (1torr = 133.322 Pa), accelerating voltage of 45 V, ion dose of $6 \times 10^{16}$ ions $cm^{-2}$, and an average beam current of 3.0 mA. The system gave a mean silver-ion charge of 2, resulting in an initial kinematic energy of 90 keV (45 × 2 keV) for each silver ion. Every 60 ° surface on the LCF specimens cylinder surface was implanted at the above nominal ion dose.

LCF tension–compression tests were carried out in a plastic strain-control mode at roughly reversed loading (stress ratio, $R$, approximately equals − 1) on a 40 kN Schenck servohydraulic materials test machine. The loading frequency ranged from 0.02–0.3 Hz with a triangular load-time function. The plastic strain was measured by a clip-on Schenck extensometer. Tensile and compression peak loads in each reversal were successively displayed and the number of reversals registered by an automatic counter. Selected cyclic stress–strain loops were documented on an $x$–$y$ recorder. During the test, the plastic strain range was controlled constantly from $3 \times 10^{-2}$–$1.2 \times 10^{-2}$.

## 3. Results and discussion

Fig. 2 shows the typical cyclic stress response to plastic strain curves obtained from the selected hysteresis loops for α-Fe with and without $Ag^+$ implantation at a dose of $6 \times 10^{16}$ ions $cm^{-2}$, where cyclic tensile stress amplitude, $\Delta\sigma/2$, is plotted against the accumulated plastic strain, $\Sigma\Delta\varepsilon_p$, at different levels of plastic strain range, $\Delta\varepsilon_p$. In the figure, $\Sigma\Delta\varepsilon_p$ is calculated as the result of fatigue life, $N_f$ (number of cycles to failure), multiplied by the plastic strain range, $\Delta\varepsilon_p$. It can be seen that the surface-modified iron displayed higher stress amplitudes in low plastic strain ranges and lower stress amplitudes in high plastic strain ranges in comparison with the unmodified iron. During the first few cycles, both the materials were observed to exhibit cyclic hardening in tension and compression reversals. This means that all the cyclic loadings controlled by the selected plastic strain ranges in the initial cycling stage had a tendency to densify dislocations in the materials. Fig. 2 also shows that with an increase of plastic strain range, the amounts of accumulated plastic strain required for the material to undergo saturation before fracture, decreased. In this paper, saturation stress amplitude, $\Delta\sigma_s/2$, is defined as the cyclic stress amplitude at half fatigue life.

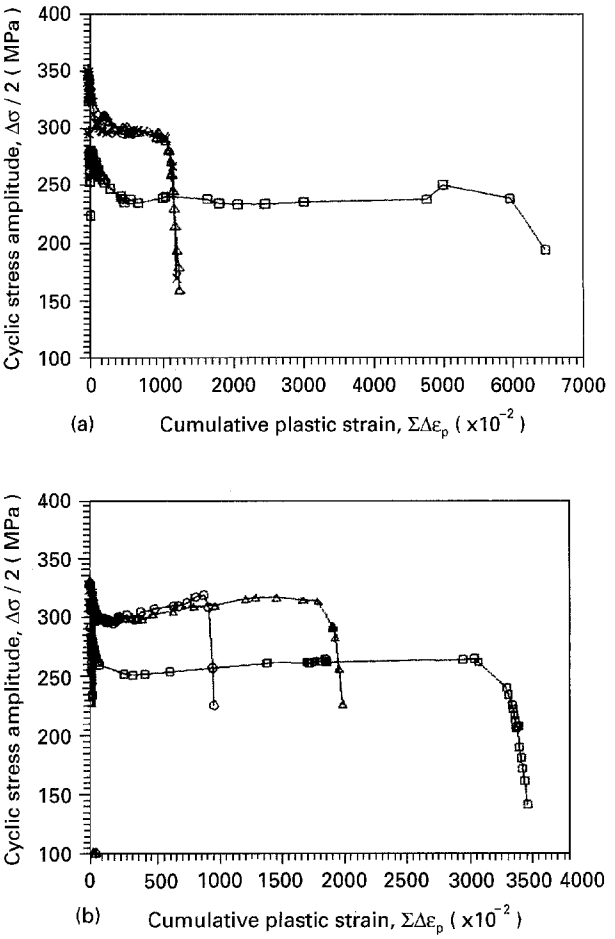


*Figure 2* Cyclic stress response at different plastic strain ranges for annealed α-iron (a) without and (b) with silver-ion implantation, see text for details. Plastic strain range: (a) (△) $6.2 \times 10^{-3}$, (×) $7.7 \times 10^{-3}$, (□) $3.0 \times 10^{-3}$; (b) (□) $5.5 \times 10^{-3}$, (△) $8.3 \times 10^{-3}$, (○) $1.1 \times 10^{-2}$.

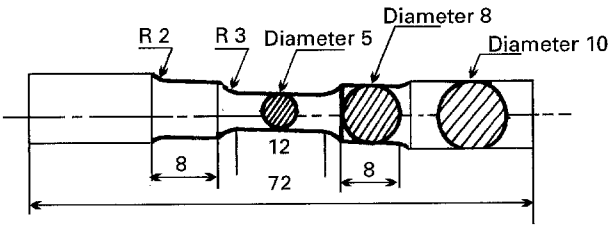


*Figure 1* Geometry and dimensions (in mm) of LCF specimens.

Further measurement of saturation stress as a function of plastic strain range yielded the so-called cyclic stress–strain (CSS) curves shown in Fig. 3, where both the CSS curves for the modified and unmodified iron have been best fit. For the unmodified iron, the CSS curve follows

$$\Delta\sigma_s/2 = 84.9 \times \ln(\Delta\varepsilon_p) + 719.9 \quad (1)$$

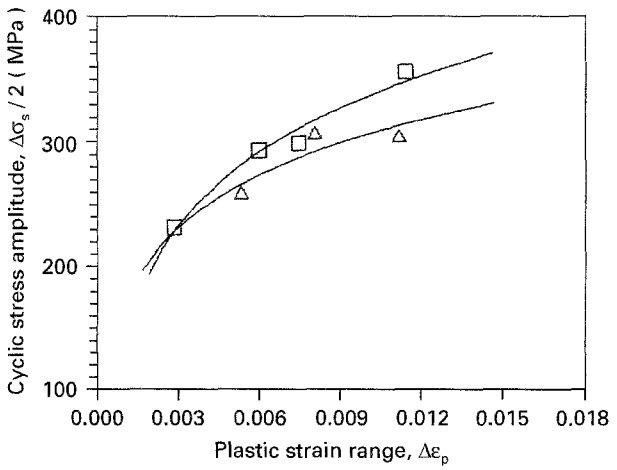


*Figure 3* CSS curves based on the data obtained from Fig. 2, see text for details. (△) Implanted, $\Delta\sigma_s/2 = 60.2\ln(\Delta\varepsilon_p) + 576.9$; (□) unimplanted, $\Delta\sigma_s/2 = 84.9\ln(\Delta\varepsilon_p) + 719.9$.

For the 90 keV, $6 \times 10^{16}$ ions $cm^{-2}$ $Ag^+$-modified iron, the curve function is

$$\Delta\sigma_s/2 = 60.2 \times \ln(\Delta\varepsilon_p) + 576.9 \qquad (2)$$

From Fig. 3, both curves are seen to go positively with diminished slopes, meaning again that the materials underwent a hardening stage as a result of lattice-defects multiplication during cyclic loading. But the unimplanted iron exhibited a higher cyclic hardening rate than the implanted iron throughout the strain ranges used. The other prominent difference that can be noted is that below a critical plastic strain-range value, the as-implanted iron maintained a higher saturation stress level, and the material behaved in a more cyclic hardening manner than the unmodified material. This implies that the silver-ion implanted substrate had already obtained a more strengthened microstructure than the pure iron before the LCF tests. Brown [20] found a correlation between the saturation stress for cyclic loading and the onset of stage III work-hardening stress for monotonic tensile loading. So in our selected LCF strain range, it would be reasonable to equate the CSS curve for iron to the monotonic true stress–strain curve surpassing the yield point, and it could be deduced that the implanted iron was cyclically hardened in this low strain range. When the strain range was higher than the above critical value, the modified and the unmodified irons behaved in the reverse way. In this case, the former exhibited a cyclic softening compared with the latter, meaning that the pure iron had developed a lattice-defect microstructure with a strength higher than the modified iron. The critical values for plastic strain range and stress amplitude at the cross-point of the two CSS curves can be calculated as $3.06 \times 10^{-3}$ and 228 MPa, respectively, based on Equations 1 and 2.

Detailed study of the CSS curve slopes in Fig. 3 reveals that, in contrast to the larger slope for pure iron, the saturation stress for implanted iron increases steadily and slowly with increase of the plastic strain range, giving a smooth, increased CSS curve. Generally, annealed metals have a low dislocation and vacancy density. The reason materials soften or harden is believed to be related to the nature and stability of the dislocation substructure of the material [21]. The high increase of the hardening rate for the annealed iron might originate from a quick dislocation multiplication in the "clear" crystal when cyclic loading was exerted. The implanted iron is believed to have obtained a substructure harder than the initial annealed iron before LCF tests. This strengthening effect on the silver-implanted iron must have resulted from the implantation. Radiation-induced defects in crystal lattices are a general occurrence during ion implantation. When energetic ions impinge on a crystal, atoms are displaced from their lattice positions. The collision events happening in the collisional cascades can produce single or clustered vacant atomic sites and displaced atoms resting at interstitial sites [22]. In such radiation defects (vacancies, interstitials, and dense clusters of vacancies or interstitials formed as a result of the nuclear displacements within each ion cascade), if disturbed by a thermal activation process at finite temperatures, the interstitials may become mobile and will migrate becoming trapped and annihilated at sinks such as vacancies, or clustering; the vacancies might agglomerate to form defect clusters which, in turn, might collapse to form dislocation loops. It is believed and also verified by our simulation of collisional cascades in silver implantation into iron, that silver implantation has induced in the substrate lattices just such a radiation defect pre-substructure, whose strength is higher than the pure iron before the LCF tests. Also, at our medium–high ion dose, intersection of dislocation loops to form dense dislocation networks is expected. Such pre-hardened iron undoubtedly possessed a stronger fatigue strength to resist fatigue damage. Respective simulations of 100 silver- and 100 silicon-ion implantations into iron at 90 keV demonstrated that the vacancy yield by each silver and silicon ion averages 2547 and 2204, respectively. This is evidence for the general rule that heavy ions can produce more defects than light ions during implantation. So, silver is very efficient in achieving radiation-defect hardening in iron. TEM investigation verified that dislocation networks had formed by a similar room-temperature ion implantation into iron by 90 keV Pd at $6 \times 10^{16}$ ions $cm^{-2}$ [23].

One of the most important aspects that should be noted is that the stability of the metastable radiation-induced defects in implantation is a decisive factor affecting the material's behaviour during service. When disturbed by a mechanical activation process as in fatigue loading, the mobility of vacancies and dislocations might be increased, defects might be annealed out as a result of a dynamically-promoted process or enhanced diffusion process, resulting from self-heating by lattice friction. As a result, the defect density might be decreased and the strength of the surface lowered. This mechanism is proposed to explain the cyclic softening of silver-implanted iron at high plastic strain range, Fig. 3.

Super solid-solution of silver in iron is the other mechanism to strengthen the iron surface by implantation. Although they are immiscible in each

other in the high-temperature liquid state or in the low-temperature solid state, ion implantation can still inject silver into the iron lattice by force. Our previous calculation concluded that for 90 keV $Ag^+$-implanted iron, each projected $Ag^+$ can deposit an average energy of 1300 eV when penetrating a lattice-parameter ($a_0 = 0.289$ nm) spacing in bcc α-iron, which is sufficiently high to debond two neighbouring iron atoms in the lattice (the binding energy for iron atoms is about 705 eV). Therefore, a super-substitutional solid solution of silver in iron might be formed during implantation. Substitutional solid solution of palladium in α-Fe has been formed before by Follstaedt and Knapp [23]. It is conceivable that ion-implantation produced solid-solution hardening is more effective at high ion doses.

In order to establish the traditional Coffin-Manson relationship

$$\Delta\varepsilon_p = \varepsilon_f' (N_f)^c \quad (3)$$

where $\varepsilon_f'$ is the fatigue ductility coefficient and $c$ the fatigue ductility exponent, three to four virgin LCF specimens were cycled to fracture. Fig. 4 gives the Coffin–Manson plots of plastic strain range versus life for the modified and unmodified polycrystalline iron. The material constants $\varepsilon_f'$ and $c$ in Equation 3 have been calculated by linear regression analysis for unimplanted and implanted iron. So the $\Delta\varepsilon_p$–$N_f$ curves for unimplanted and implanted iron can be given, respectively, as

$$\Delta\varepsilon_p = 0.076\ (N_f)^{-0.32} \quad \text{unimplanted iron} \quad (4)$$

$$\Delta\varepsilon_p = 0.216\ (N_f)^{-0.42} \quad \text{implanted iron} \quad (5)$$

Fig. 4 demonstrates that the $\Delta\varepsilon_p$–$N_f$ curve for implanted iron has been shifted to the upper right corner with respect to that of pure iron. Thus an increase in the endurance limit strain (ELS) or life (ELL) at a certain cycle in the LCF range, can be obtained. Direct evidence for this is the elevated values of $\varepsilon_f'$ and $c$ after silver-ion implantation, an indication of the improvement in fatigue ductility. It is commonly known that fatigue is a process governed both by strength and ductility of materials. This is specifically true for LCF, in which specimens undergo a certain plastic deformation besides elastic deformation in each cycle. So, according to Coffin [24] and Manson [25], the basic strain-life function in LCF is

$$\Delta\varepsilon_t/2 = (\sigma_f'/E)(N_f)^b + \varepsilon_f'(N_f)^c \quad (6)$$

where $\Delta\varepsilon_t/2$ is the total strain amplitude, $\sigma_f'$ the fatigue strength coefficient, $b$ the fatigue strength exponent, and $E$ the Young's modulus. The first term on the right of the above equation is an elastic term, a measure of fatigue strength; the second term is a plastic term, a measure of fatigue ductility. Throughout the LCF test, comparison of the horizontal distance between two end points on the hysteresis loops with the plastic strain range width on these loops indicated that all the LCF tests had proceeded with the second term larger than the first one. It might, therefore, be deduced that in our test conditions, the greater part of the specimen's life was consumed by

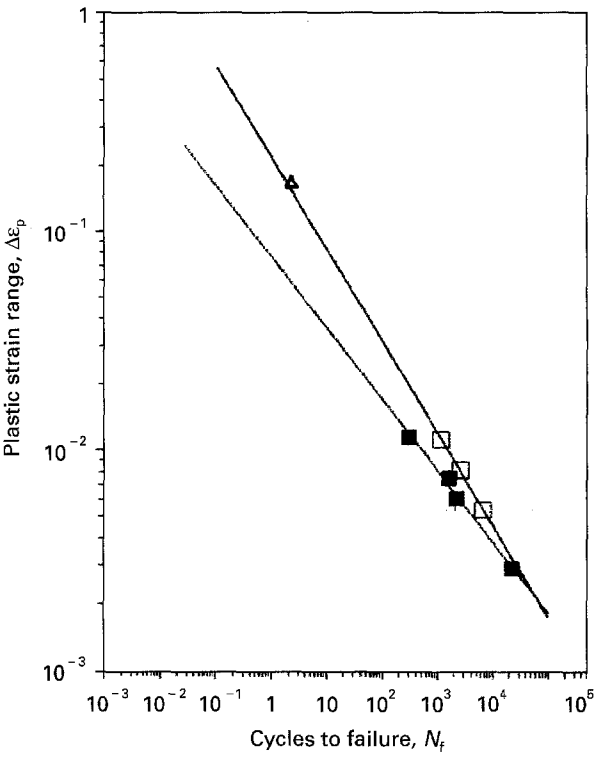


*Figure 4* Coffin–Manson plot for the cyclically deformed α-iron (■) without ($\Delta\varepsilon_p = 0.076N_f^{-0.32}$) and (□) with ($\Delta\varepsilon_p = 0.216N_f^{-0.42}$) silver-ion implantation.

cyclic plastic deformation. So, in addition to fatigue strength enhancement, fatigue ductility improvement is the other dominant mechanism for the better LCF behaviour of the iron after silver-ion implantation.

Improved ductility means improved cyclic plasticity. The dislocation plasticity of the bcc metals differs from that of fcc ones in that the cross-slip of screw dislocations in bcc metals is preferred in highly stressed conditions, while screw dislocations in fcc ones can experience a dissociation reaction into two partial dislocations separated by a stacking fault region before cross-slip occurs. Although the difference in SFE between bcc and fcc metals might be one reason for this, the virtually unique features of bcc metals, in which screw dislocations have a three-fold symmetry and a high Peierls stress, are the intrinsic mechanisms [26–29]. As a result of these specific features, the intrinsic interaction of dislocation cores with the crystal lattices in bcc metals differs from that of fcc ones. Cross-slip causes screw dislocations to migrate and annihilate each other, leading to a storage of edge dislocation dipoles and double kinks, etc. Cyclic hardening originates from the multiplication of such edge dislocation debris. The process of cross-slip is thermodynamically irreversible. Because of the ease of cross-slip in bcc metals, the deformation irreversibility and cyclic hardening rate as a result of the production of edge dipoles, are high.

One of the direct negative results from this characteristic in bcc materials is the lowered saturation stress in cyclic deformations. Our empirical evidence shows that after implantation, the CSS-curve slope has been decreased, and the fatigue ductility coefficient and exponent have both been enlarged. These factors present ready evidence for the microplasticity

improvement by implantation: the occurrence of cross-slip must have been decreased, and the reversibility of cyclic deformation increased. This might be best understood by introducing a reduced critical spacing, $h_c$, after implantation. The parameter is defined as the critical spacing separating two screw dislocations just on the point of annihilation on slip lanes [20]. A small value of $h_c$ means cross-slip will be difficult. In f c c metals, the increased fatigue property has been partially attributed to an SFE reduction after implantation [15, 16], which is also evidence of fatigue ductility improvement after implantation. Whatever explanations might be proposed, one is confirmed in our work that the cross-slip of screw dislocations in b c c α-iron has been made difficult, after which fatigue ductility improved following silver-ion implantation.

## 4. Conclusion

LCF tests on polycrystalline α-iron with and without silver-ion implantation have been conducted. It is shown that the fatigue property has been improved after ion implantation. Enhanced fatigue ductility, due to hindered or delayed cross-slip of screw dislocations after implantation, is proposed as the dominant mechanism in the LCF test condition. Strengthening due to radiation induced defects and super-solid solution is also proposed as another mechanism for the fatigue property improvement by silver-ion implantation.


## Acknowledgements

This paper forms part of the doctoral dissertation work of Hong W. Wang at DUT. Special thanks are due to Professor D.Z. Yang for his beneficial guidance. Support from the State Key Laboratory for Materials Modifications by Three Beams of DUT, and the State Key Laboratory for Fatigue and Fracture of Materials of IMR, are gratefully acknowledged.


## References


1. H. W. WANG, D.Z. YANG, W. D. SHI and S. PATU, *Scripta Metall. Mater.*, **32** (1995) 2001.
2. O. KUBASCHEWSKI (ed.), "Iron Binary Phase Diagrams" (Springer, Berlin, 1982) p. 3.
3. D. KUHLMANN-WILSDORF and C. LAIRD, *Mater. Sci. Eng.* **27** (1977) 137.
4. *Idem, ibid.* **37** (1979) 111.
5. *Idem, ibid.* **46** (1980) 209.
6. D. KUHLMANN-WILSDORF, *ibid.* **39** (1979) 127.
7. C. LAIRD, J. M. FINNEY and D. KUHLMANN-WILSDORF, *ibid.* **50** (1981) 127.
8. H. MUGHRABI, *ibid.* **33** (1978) 207
9. A. S. CHEN and C. LAIRD, *ibid.* **51** (1981) 111.
10. H. MUGHRABI, in "Proceedings of the 5th International Conference on Strength of Metals and Alloys", edited by P. HAASEN, V. GEROLD and G. KOSTORZ (Pergamon, Oxford, 1980) Vol. 3, p. 1615.
11. H. HERMAN, *Nucl. Instrum. Meth.* **182/183** (1981) 887.
12. S. T. PICRAUX and L. K. POKE, *Science* **226** (1984) 615.
13. G. K. HUBLER, L. I. SINGER and C. R. CLAYTON, *Mater. Sci. Eng.* **69** (1985) 203.
14. M. GRENNESS, M. W. THOMPSON and R. W. CAHN, *J. Appl. Electrochem.* **4** (1974) 211.
15. S. PATU, M. H. XU and Z.G. WANG, *Mater. Sci. Eng.* **A115** (1989) 323.
16. J. MENDEZ, P. VIOLAN and M. F. DENANOT, *Nucl. Instrum. Meth. Phys. Res.* **B19/20** (1987) 232.
17. D. J. MORRISON, J.W. JONES, D.E. ALEXANDER and G. S. WAS, *Metall. Trans.* **22A** (1991) 1633.
18. D. S. GRUMMON, J. W. JONES and G. S. WAS, *ibid.* **19A** (1988) 2775.
19. D. S. GRUMMON, J.W. JONES, J.M. MERIDON, G.S. WAS and L. E. REHN, *Nucl. Instrum. Meth. Phys. Res.* **B19/20** (1987) 227.
20. L. M. BROWN, *Metall. Trans.* **22A** (1991) 1693.
21. R. W. HERTZBERG, "Deformation and Fracture Mechanics of Engineering Materials", 2nd Edn (Wiley, New York, 1983).
22. J. O. STIEGLER and L.K. MANSUR, *Ann. Rev. Mater. Sci.* **9** (1979) 405.
23. D. M. FOLLSTAEDT and J. A. KNAPP, in "Laser-Solid Interactions and Transient Thermal Processing of Materials", edited by J. NARAYAN, W.L. BROWN and R.A. LEMONS (North Holland, New York, 1983) p. 745.
24. L. F. COFFIN Jr, *Trans. ASME* **76** (1954) 931.
25. S.S. MANSON, paper presented at the Heat Transfer Symposium, University of Michigan Engineering Research Institute (1953) p. 9.
26. B. SESTAK, in "Proceedings of the 5th International Conference on Strength of Metals and Alloys", edited by P. HAASEN, V. GEROLD and G. KOSTORZ, (Pergamon, Oxford, 1980) Vol. 3, p. 1461.
27. A. SEEGER and B. SESTAK, *Scripta Metall.* **5** (1971) 875.
28. V. VITEK, *Cryst. Latt. Defects* **5** (1974) 1.
29. L. P. KUBIN and F. LOUCHET, *Philos. Mag.* **38** (1978) 205.



*Received 22 December 1994*
*and accepted 2 May 1995*